

VOIC: Visible–Occluded Decoupling for Monocular 3D Semantic Scene Completion

Zaidao Han, Risa Higashita, Jiang Liu, *Senior Member, IEEE*

Abstract—Camera-based 3D Semantic Scene Completion (SSC) is a critical task for autonomous driving and robotic scene understanding, aiming to infer a complete 3D volumetric representation of both semantics and geometry from a single image. Existing methods typically focus on end-to-end 2D-to-3D feature lifting and voxel completion, yet they often overlook the interference between high-confidence visible-region perception and low-confidence occluded-region reasoning caused by single-image input, which can lead to feature dilution and error propagation. To address these challenges, we introduce an offline Visible Region Label Extraction (VRLE) strategy that explicitly separates and extracts voxel-level supervision for visible regions from dense 3D ground truth, thereby purifying the supervisory space for the two complementary sub-tasks of visible-region perception and occluded-region reasoning. Building upon this, we propose the Visible–Occluded Interactive Completion Network (VOIC), a novel dual-decoder framework that explicitly decouples SSC into visible-region semantic perception and occluded-region scene completion. VOIC first constructs a base 3D voxel representation by fusing image features with depth-derived occupancy. The Visible Decoder then focuses on generating high-fidelity geometric and semantic priors, while the Occlusion Decoder leverages these priors along with cross-modal interaction to perform coherent global scene reasoning. Extensive experiments on the SemanticKITTI and SSCBench-KITTI360 benchmarks demonstrate that VOIC outperforms existing monocular SSC methods in both geometric completion and semantic segmentation accuracy, achieving state-of-the-art performance. The code and pre-trained models are available at: <https://github.com/dzrdzrdzr/VOIC>.

Index Terms—Semantic Scene Completion, Visible–Occluded Decoupling, Autonomous Driving, Visible Region Label Extraction

I. INTRODUCTION

3D Semantic Scene Completion (SSC) aims to infer the complete 3D geometry and semantic structure of a scene from partial visual observations, such as monocular or stereo images. As a fundamental task in scene understanding, SSC provides dense and structured 3D representations of the surrounding environment, serving as a crucial bridge between

This work was supported in part by the National Key R&D Program of China (No. 2024YFE0198100) and the Shenzhen Medical Research Funds (Grant No. D2402014).

Zaidao Han and Risa Higashita are with the Research Institute of Trustworthy Autonomous Systems, Southern University of Science and Technology, Shenzhen 518055, China, and also with the Department of Computer Science and Engineering, Southern University of Science and Technology, Shenzhen 518055, China (emails: 12445017@mail.sustech.edu.cn; risa@mail.sustech.edu.cn).

Jiang Liu is with the Research Institute of Trustworthy Autonomous Systems, and the Department of Computer Science and Engineering, Southern University of Science and Technology, Shenzhen 518055, China; the School of Computer Science, University of Nottingham Ningbo China, Ningbo 315100, China; and the Department of Electronic and Information Engineering, Changchun University, Changchun 130022, China (email: liuj@sustech.edu.cn).

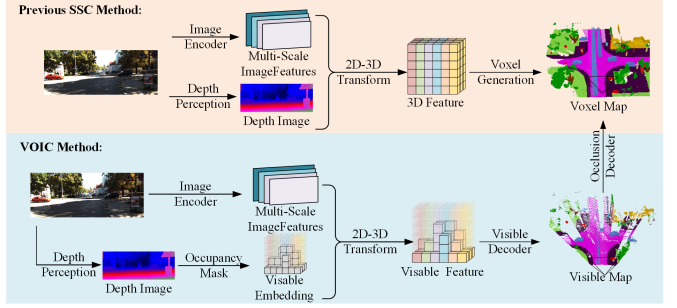


Fig. 1. Overview of the proposed VOIC framework. Unlike conventional semantic scene completion (SSC) methods that directly supervise with full ground-truth labels, VOIC adopts an explicitly decoupled progressive process. 2D features are first lifted to 3D via cross-modal feature fusion. The Visible Decoder (VD) processes observed regions, and the Occlusion Decoder (OD) leverages normalized VD features as priors to reconstruct the complete 3D scene.

perception and reconstruction. Accurate SSC is critical for numerous downstream applications, including autonomous driving, robotic navigation, and mixed reality [1]–[3].

Traditional LiDAR-based SSC methods [2], [4], [5] achieve high geometric accuracy due to high-quality 3D sensors. However, they suffer from high sensor costs, sparse points at long distances, and limited scalability for large-scale deployment. These limitations have driven research on camera-based SSC, which leverages dense image information to recover high-resolution 3D geometry and semantics without relying on expensive hardware [1].

Most existing vision-based SSC methods follow a standard pipeline: first extract 2D features, then project to 3D voxels, and finally decode the voxels. In this paradigm, 2D features extracted by a backbone network are lifted into the 3D voxel space, and decoders predict occupancy and semantic labels. To reduce depth ambiguity, many methods introduce auxiliary depth estimation [6], [7] to provide coarse geometric priors within the camera frustum. Despite these advances, monocular SSC remains highly challenging due to severe occlusions, complex spatial dependencies, and uneven information density between visible and occluded regions.

Notably, many vision-based SSC methods rely on multi-frame sequences to expand the coverage of occluded regions and ease the difficulty of predicting hidden geometry. In contrast, single-frame monocular SSC lacks temporal information, which substantially increases the challenge of accurately reconstructing occluded voxels.

Crucially, SSC can be regarded as two complementary sub-tasks: (1) semantic segmentation of camera-visible voxels, and (2) semantic completion of occluded voxels. Existing methods,

such as MonoScene [1] and VoxFormer [6], typically process all voxels in a unified manner, ignoring the distinction between observed and unobserved regions. This unified decoding approach fails to account for differences in voxel uncertainty, often leading to inaccurate reconstruction of visible regions and propagating errors to occluded areas. Explicitly separating these tasks can provide more interpretable supervision and improve learning stability.

To address this challenge under single-frame monocular input, we propose the Visible–Occluded Interactive Completion Network (VOIC), which decomposes SSC into two stages: visible region perception and occluded region prediction. By explicitly distinguishing voxels directly observed from those occluded, VOIC can achieve structured and accurate semantic scene completion without relying on historical frames or multi-view inputs.

To further provide structured supervision for visible voxels, we introduce Visible Region Label Extraction (VRLE), an offline label generation strategy to identify which voxels are directly observable from the camera viewpoint. VRLE generates visible voxel labels from the full 3D annotations, achieving a clean separation between visible and occluded voxels. This approach enhances supervision of visible voxels and provides structured guidance for subsequent completion.

Building upon VRLE, VOIC employs a dual-decoder design:

- 1) The Visible Decoder (VD) is trained with VRLE-generated visible labels, accurately reconstructing the geometry and semantics of observed voxels.
- 2) The Occlusion Decoder (OD) interacts with the VD, utilizing normalized visible features as spatial-semantic priors and providing global contextual feedback to refine visible-region predictions. The OD is trained with the complete 3D scene labels, leveraging these priors to holistically infer the full scene, producing the final, complete voxel prediction.

To ensure the decoders can establish robust and high-precision geometric priors and achieve efficient feature interaction, VOIC integrates multi-level positional encoding and an adaptive feature interaction module. During 3D projection, the Visible Embedding Feature Constructor (VEFC) enriches 2D features with spatial geometric information. VEFC utilizes a dynamic learnable sampling mechanism, effectively mitigating the feature dilution caused by depth errors in traditional fixed projection methods. During voxel decoding, on one hand, hierarchical encoding captures the relative spatial relationships between voxel features and position queries. On the other hand, to ensure the establishment of high-precision instance boundaries and semantic priors, and to support instance-level perception for capturing critical discrete objects in the scene, our adaptive feature interaction module allows voxel features to query information between 2D images and 3D priors. It is worth noting that the purpose of OD reusing cross-modal interaction is to correct potential geometric errors in the VD prior, ensuring the highest fidelity of the final global reconstruction result.

Extensive experiments on SemanticKITTI [8] and SSCBench-KITTI-360 [9] demonstrate that VOIC consistently

outperforms existing vision-based SSC methods across multiple metrics, achieving state-of-the-art performance in geometric completion and semantic consistency. The main contributions of this work are summarized as follows:

- 1) We propose VOIC, a novel monocular SSC framework that explicitly distinguishes visible and occluded voxels through the Visible Region Label Extraction (VRLE) strategy. We design a dual-decoder architecture (VD and OD) that enables collaborative reasoning: VD establishes robust visible priors, and OD leverages these priors to infer the complete scene, following a visible-first, occlusion-second paradigm.
- 2) We introduce the Visible Embedding Feature Constructor (VEFC) and multi-level positional encoding mechanism to systematically enhance voxel feature geometric discriminability and semantic alignment, providing a solid geometric foundation for VD/OD collaborative reasoning.
- 3) We conduct extensive experiments on SemanticKITTI and SSCBench-KITTI-360 to validate the effectiveness of VOIC. Results demonstrate superior performance over existing monocular SSC methods.

II. RELATED WORK

3D Semantic Scene Completion (SSC) aims to infer a complete volumetric representation of a scene, encompassing both the geometric structure and semantic labels of observed and occluded regions. Existing methods can be broadly categorized into those relying on native 3D sensor inputs and those adopting a vision-centric approach.

A. 3D Input-based Approaches

Early SSC methods leveraged native 3D data for high-fidelity reconstruction. The pioneering work, SSCNet [10], introduced SSC for indoor RGB-D scenes. Subsequent methods, such as 3DSketch [11], the approach by Li et al. [12], and the Cascaded Context Pyramid Network (CCPNet) [13], adopted the Truncated Signed Distance Function (TSDF) to better guide the prediction of geometry and semantics.

The emergence of large-scale outdoor datasets, such as SemanticKITTI [8] and OpenOccupancy [14], subsequently catalyzed the development of methods tailored for outdoor environments. A common strategy in this domain is to directly process LiDAR point clouds. For instance, LMSCNet [15] utilizes a 2D UNet to extract Bird’s-Eye View (BEV) features from sparse scans, which are then unrolled along the height dimension to complete the 3D scene. JS3C-Net [16] proposes a sparse single-sweep segmentation framework with contextual shape priors and leverages multi-frame LiDAR aggregation to convert sparse scans into dense representations.

o leverage complementary information from images and LiDAR, recent methods focus on multi-modal fusion. Chang et al. [17] address unreliable image features and modality trade-offs by introducing a weakly-supervised loss, attention-based feature fusion, and confidence-aware late fusion. IPVoxelNet [18] maps images and point clouds into a unified voxel space, independently learns geometric and semantic features,

and uses cross-modal knowledge distillation to enhance scene understanding.

While 3D input-based methods achieve remarkable accuracy, their dependency on expensive sensors like LiDAR limits practical scalability. This constraint has motivated a parallel line of research into vision-centric methods, which seek to infer complete 3D scenes from low-cost, readily available monocular or multi-view images.

B. Visual-Centric Approaches

Vision-centric SSC methods address the challenge of reconstructing 3D scenes from images. The monocular SSC pipeline was largely established by MonoScene [1], which lifts 2D image features into a 3D frustum to generate dense voxel representations. Early innovations primarily focused on enhancing the 3D decoder: OccFormer [19] provides efficient, long-range encoding for voxel features; NDC-scene [20] projects 2D features into Normalized Device Coordinate (NDC) space to recover depth; and TPVFormer [21] represents 3D space with tri-perspective views and uses Transformers to capture spatial dependencies. HASSC [22] tackles the class imbalance issue via a hard sample-aware training strategy that dynamically selects challenging voxels for refinement.

A core challenge in monocular SSC is depth ambiguity. VoxFormer [6] systematically addresses this by first generating sparse depth estimates and then using deformable attention to propagate and densify contextual features. Beyond geometry, instance-level reasoning has also been integrated to boost performance. Symphonies [7] employs serial instance propagation attention to model instance semantics and reduce occlusion errors, while Xiao et al. [23] propose an instance-aware framework that fuses mask-derived cues via a dedicated attention module.

The field has recently seen significant advances through multi-modal fusion and temporal modeling. MixSSC [24] combines sparse features from forward projection with dense depth priors from backward projection. HTCL [25] introduces hierarchical temporal context learning for better consistency. CurriFlow [26] leverages optical flow and curriculum learning, and CF-SSC [27] extends the perceptual range via pseudo-future frame prediction.

Architectural innovations continue to push the boundaries. FoundationSSC [28] proposes a dual-decoupling framework for separate semantic and geometric refinement. MV-Former [29] utilizes a UNet-like decoder with Mix-Voxel attention, VFG-SSC [30] adopts a semi-supervised approach to leverage 2D foundation models, SPHERE [31] jointly models semantics and physics with voxels and Gaussians, and MARE [32] introduces a memory bank to complete unseen regions.

In summary, while many vision-centric methods mitigate occlusion by leveraging multi-frame inputs, this approach is inapplicable to the single-image setting. Precisely to address this gap, we propose the VOIC. Our method explicitly decouples the task into “visible region perception” and “occluded region prediction” stages, enabling structured and accurate completion from a single monocular image without historical data.

III. METHODOLOGY

A. Overview

We introduce VOIC, a unified framework designed to explicitly decouple the monocular 3D Semantic Scene Completion (SSC) task into visible-region perception and holistic scene reconstruction. Formally, given a single RGB image $I^{rgb} \in \mathbb{R}^{H_{img} \times W_{img} \times 3}$ as input, the objective is to predict the complete scene geometry and semantics, represented as a voxel grid \hat{Y} , which approximates the ground truth $Y \in \mathbb{R}^{H \times W \times D \times N_c}$. This is formulated as learning a network Θ such that $\hat{Y} = \Theta(I^{rgb})$. The VOIC architecture follows a progressive, visible-to-complete processing paradigm.

Prior to training, we employ an offline Visible Region Label Extraction (VRLE) strategy (Sec. III-B) to derive explicit visibility supervision from the complete ground-truth annotations, providing a principled foundation for decoupled learning.

During the forward pass, as illustrated in Figure 2, the pipeline first employs the Visible Embedding Feature Constructor (VEFC) (Sec. III-C) to lift 2D image features into a unified 3D volumetric representation. Specifically, VEFC leverages a ResNet-50 backbone [33] to extract multi-scale image features, which are then fused with depth-informed positional encodings. To strengthen the coupling between image features and occupancy information, we adopt a DETR-style attention module [34], that dynamically processes occupancy cues within the 3D voxel space.

These 3D features are subsequently processed by the Visible Decoder (VD) (Sec. III-D) to accurately reconstruct the geometry and semantics of the observable surfaces. The VD employs instance-aware attention to emphasize target regions, thereby strengthening the coupling between image cues and their corresponding volumetric features. Building upon the VD’s high-fidelity predictions, the Occlusion Decoder (OD) (Sec. III-E) uses these results as spatial-semantic priors to infer both the visible and the complete 3D scene, ensuring a coherent and holistic reconstruction.

Finally, the segmentation head incorporates an ASPP module [35] to aggregate multi-scale context, and uses transposed convolutions to produce per-voxel logits for the final semantic prediction.

Subsequent sections describe the VRLE preparation, VEFC design, dual-decoder interaction, and the specialized loss that forms the overall training objective.

B. Visible Region Label Extraction (VRLE)

Standard SSC datasets (e.g., SemanticKITTI [8]) provide complete 3D semantic annotations but inherently lack explicit distinctions between visible and occluded voxels. This uniform supervision fails to account for the fundamentally different nature of visible perception versus occluded reasoning. To solve this, we introduce VRLE, an offline label generation strategy that provides unambiguous supervision for the proposed Visible Decoder by performing a visibility-aware projection. The VRLE process begins with *Voxel Instantiation and Geometric Projection*. Given the complete ground-truth semantic voxel grid $Y \in \mathbb{R}^{X \times Y \times Z}$, we first extract the set of occupied voxels $\mathcal{V} = v_i \mid Y_i \neq 0$. For each voxel v_i , we define its structure by

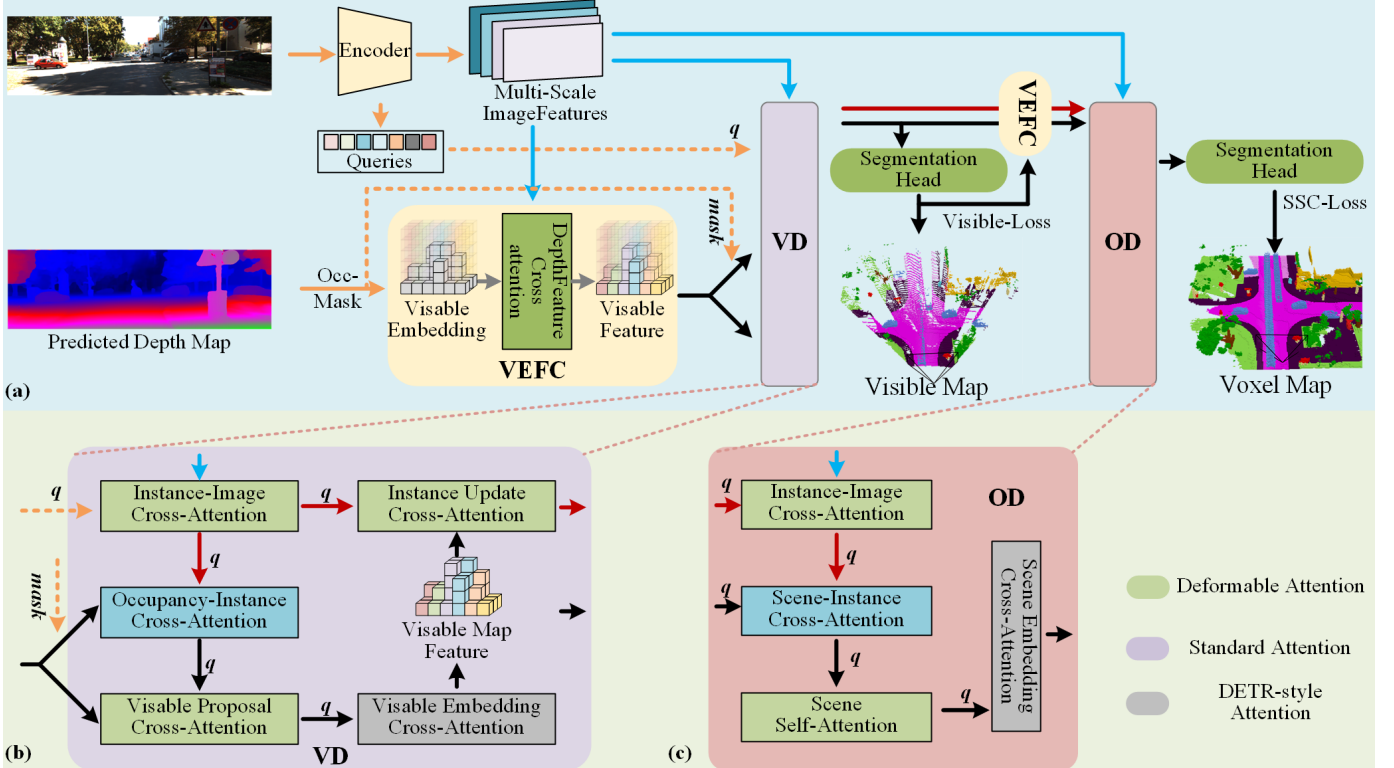


Fig. 2. Overall architecture of the VOIC framework. (a) The model follows a progressive visible-occluded paradigm that decouples the monocular 3D Semantic Scene Completion (SSC) task. The Visible Embedding Feature Constructor (VEFC) lifts 2D image features into 3D and fuses them with depth-derived occupancy to form a unified volumetric representation. (b) The Visible Decoder (VD) predicts the geometry and semantics of the observed regions under explicit visible-region voxel supervision. (c) The Occlusion Decoder (OD) takes the normalized visible features from VD as spatial-semantic priors and completes the full 3D scene structure.

eight vertices $\mathcal{P}_i^{vox} \in \mathbb{R}^{8 \times 3}$. Since visibility is determined by the voxel's actual surfaces rather than its center, representing each voxel with eight vertices allows explicit modeling of surface-level occlusion. To simulate the imaging process and establish correspondence between the 3D voxel structure and the 2D input image, each voxel vertex \mathbf{p}^{vox} is transformed to the camera coordinate system \mathbf{p}^{cam} and then projected onto the image plane using the standard pin-hole camera model. This pipeline uses the voxel-to-world transformation $\mathbf{T}_{v \rightarrow w}$, the camera extrinsic parameters $[\mathbf{R}|\mathbf{t}]$, and the intrinsic matrix \mathbf{K} , and is formally defined by:

$$\mathbf{p}^{cam} = \mathbf{R}(\mathbf{T}_{v \rightarrow w} \cdot \mathbf{p}^{vox}) + \mathbf{t}, \\ u = \text{round}\left(f_x \frac{x}{z} + c_x\right), \quad v = \text{round}\left(f_y \frac{y}{z} + c_y\right), \quad (1)$$

where $\mathbf{p}^{cam} = [x, y, z]^\top$ is the point in the camera frame, f_x, f_y are the focal lengths, and (c_x, c_y) is the principal point. The resulting pixel coordinates (u, v) define the 2D polygonal projection Π_i for each voxel v_i .

Identifying truly visible voxels requires eliminating depth ambiguity due to occlusions. Since traditional ray-casting is prohibitively slow for dense voxel grids, we employ a *Vectorized Sparse Rasterization pipeline enhanced with Z-buffering*. For computational efficiency, we first perform Sparse Bounding-Box Sampling: for each projected voxel Π_i , we compute its 2D Axis-Aligned Bounding Box (AABB) \mathcal{B}_i and generate a sparse grid of candidate pixels \mathcal{S}_i within \mathcal{B}_i

using a sampling stride δ (e.g., $\delta = 4$). Next, in the Inclusion Verification and Depth Interpolation stage, we decompose the cube's projected volume into its six quadrilateral faces. A vectorized cross-product test is employed to determine if a candidate pixel $p \in \mathcal{S}_i$ falls within any projected face. For every validated pixel p , we calculate its precise depth d_p through robust linear interpolation of the face vertices' depths, explicitly handling degenerate projection cases to ensure numerical stability. We maintain a global depth buffer $\mathcal{Z} \in \mathbb{R}^{H_{img} \times W_{img}}$ to record the minimum depth. The visibility mask is generated by the following rule: a voxel v_i is marked as visible if its depth is the smallest at any covered pixel location (u, v) :

$$v_i \in \mathcal{V}_{vis} \iff \exists (u, v) \in \Pi_i, \text{ s.t. } d_{u,v}^{(i)} = \min_{j \in \mathcal{V}}(d_{u,v}^{(j)}), \quad (2)$$

where $d_{u,v}^{(j)}$ is the interpolated depth of voxel v_j at pixel (u, v) . Finally, VRLE produces a binary visibility mask $\mathbf{M}_{vis} \in \{0, 1\}^{X \times Y \times Z}$. The ground truth is then strategically decoupled to derive the visible targets $\mathbf{Y}_{vis} = \mathbf{Y} \odot \mathbf{M}_{vis}$. These \mathbf{Y}_{vis} provide dedicated supervision for the Visible Decoder, while the complete ground truth \mathbf{Y} is used to supervise the final prediction of the Occlusion Decoder, ensuring holistic scene understanding.

C. Visible Embedding Feature Constructor (VEFC)

First, using the depth distribution \mathbf{D}_{pre} obtained from the depth prediction module, we transform pixel coordinates into world coordinates through the camera parameters to construct a binary occupancy mask $\mathbf{M} \in \{0, 1\}^{X \times Y \times Z}$ within the 3D voxel space. This mask is activated only at voxel locations intersected by the projected depths, effectively filtering out uninformative free space.

For the valid voxels indicated by the mask \mathbf{M} , we initialize their content features $\mathbf{Q}_{content}$ as zero vectors. These zero vectors are then fused with the image features \mathbf{F}_{2D} , where $\mathbf{F}_{2D} = \text{Backbone}(I^{rgb})$, through a Deformable Attention module (DeformAttn) [34]. In this process, the 3D geometric positional encoding \mathbf{S}_{pos} is added to the content-free queries to form positional queries, which guide the attention mechanism to attend to the corresponding regions in the image features.

$$\mathbf{F}_{voxel} = \text{DeformAttn}(\mathbf{Q}_{content} + \mathbf{S}_{pos}, \mathcal{P}(\mathbf{S}_{pos}), \mathbf{F}_{2D}) \quad (3)$$

where \mathcal{P} denotes the 3D-to-2D projection function. In the Deformable Attention module, the voxel queries—augmented with geometric positional encoding—attend to their corresponding regions in the image feature map. This mechanism ensures that the resulting voxel features are directly grounded in the explicit correspondence between 3D geometry and image appearance under the current view, thereby preventing the “hallucinated” responses that often arise from free-form learnable queries in occluded or complex areas. Finally, the generated sparse features are scattered back into the dense blank grid to form the initial scene embedding.

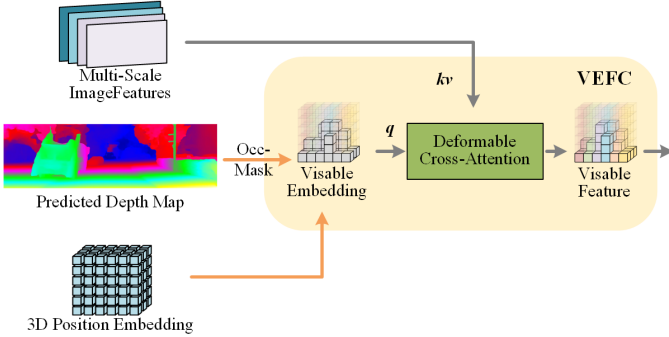


Fig. 3. Sparse Voxel Feature Initialization. The VEFC module creates a geometry-driven 3D representation using a zero-initialized query. An occupancy mask sparsifies the structure, while 3D positional encoding enables precise localization. Deformable Attention then aggregates 2D image features into the visible voxels.

D. Visible Decoder (VD)

As shown in Fig. 2(b), the Visible Decoder (VD) is the core component of the VOIC framework, responsible for achieving high-precision semantic perception within the visible region. By leveraging the two-dimensional image features \mathbf{F}_{2D} , instance queries \mathbf{Q}_{inst} , and the initial 3D scene embedding \mathbf{F}_{vis} constructed by VEFC combined with the binary occupancy mask \mathbf{M} , a reliable 3D structure and semantic prior \mathbf{F}_{vis}^{VD} is established.

First, the instance queries \mathbf{Q}_{inst} interact with the multi-scale image features \mathbf{F}_{2D} via the *Instance-Image Cross Attention* mechanism:

$$\mathbf{Q}'_{inst} = \text{DeformAttn}(\mathbf{Q}_{inst}, \mathbf{R}_{2D}, \mathbf{F}_{2D}) \quad (4)$$

where \mathbf{R}_{2D} are the 2D image instance reference points. This step ensures that the instance queries effectively capture semantic cues related to the target instances from the 2D image, serving as the bridge that links image features with the subsequent 3D representations, thereby producing the enhanced instance query \mathbf{Q}'_{inst} .

Subsequently, VD refines voxel features in the visible region by using the visibility mask \mathbf{M} to remove invisible areas and retain only the effective embeddings \mathbf{E}_{vis} .

$$\mathbf{E}_{vis} = \text{Flatten}(\mathbf{F}_{vis}) \mid \mathbf{M} \quad (5)$$

The flattened visible voxel features \mathbf{E}_{vis} (as Query) undergo standard Cross Attention computation with the enhanced instance queries \mathbf{Q}'_{inst} (as Key/Value) in the *Occupancy-Instance Cross Attention* step. This injects the instance semantic information from the 2D perspective into the 3D visible voxel features, achieving cross-modal information integration. The refined \mathbf{E}_{vis} subsequently interacts with the complete flattened voxel features $\text{Flatten}(\mathbf{F}_{vis})$ in the *Visible Proposal Cross Attention* mechanism. By leveraging the global 3D scene context, this enhances the structural consistency and local semantic expression ability of the visible voxel features, thereby establishing a strong structural prior. Finally, the *Scene Embedding Cross-Attention* is instantiated as a DETR-style attention module. Distinct from standard attention mechanisms, it applies independent linear projections to the content and positional encodings of the queries and keys prior to fusion. Through this decoupled design, the entity features \mathbf{E}_{vis} and class embeddings \mathbf{C}_{vd} serving as scene-level features are able to achieve more robust interaction. Finally, the module generates \mathbf{E}'_{vis} .

The sparse features of the visible region \mathbf{E}'_{vis} refined through multiple stages are remapped back into the dense 3D grid via the IndexBack operation, forming the final visible region prior \mathbf{F}_{vis}^{VD} :

$$\mathbf{F}_{vis}^{VD} = \text{IndexBack}(\mathbf{E}'_{vis}, \mathbf{M}) \quad (6)$$

In the final *Instance Update Cross-Attention* module, the instance query \mathbf{Q}'_{inst} first interacts with the updated visible-region features \mathbf{F}_{vis}^{VD} through 3D Deformable Cross Attention, yielding the refined query \mathbf{Q}''_{inst} . This updated query fuses the predicted visible-voxel features and is subsequently fed into the Occlusion Decoder (OD) to guide the reconstruction of the complete voxel scene.

$$\mathbf{Q}''_{inst} = \text{DeformAttn}(\mathbf{Q}'_{inst}, \mathbf{R}_{3D}, \text{Flatten}(\mathbf{F}_{vis}^{VD})) \quad (7)$$

where \mathbf{R}_{3D} are the 3D voxel positions. The VD module ultimately outputs the refined voxel features \mathbf{F}_{vis}^{VD} , the enhanced instance queries \mathbf{Q}_{inst}'' , and produces the visible-region semantic voxel prediction \hat{Y}_{vis} through the segmentation head. During the training phase, \mathbf{F}_{vis}^{VD} is used for semantic prediction of the visible region and is explicitly supervised by the visible labels \mathbf{Y}_{vis} derived from VRLE, ensuring the

model establishes accurate structural and semantic priors in the visible area.

E. Occlusion Decoder (OD)

Based on the semantic predictions \dot{Y}_{vis} and the refined 3D voxel features \mathbf{F}_{vis}^{VD} produced by the Visible Decoder (VD), the Occlusion Decoder (OD) aims to complete the full 3D scene by propagating structural and semantic priors into the unobserved regions. To further strengthen the guidance effect of VD, the OD additionally reuses the VEFC mechanism, where the VD-refined voxel features \mathbf{F}_{vis}^{VD} serve as the content queries and are fused with the multi-scale image features \mathbf{F}_{2D} through deformable attention. This design reinforces the visible-region priors encoded in \mathbf{F}_{vis}^{VD} while preventing the generation of hallucinated features in occluded space.

As illustrated in Fig. 2(c). This module utilizes the visible voxel embeddings \mathbf{F}_{vis}^{VD} refined by the VD, the instance queries $\mathbf{Q}_{inst}^{''}$, and the multi-scale image features \mathbf{F}_{2D} to propagate semantic information into occluded regions, ensuring accurate 3D structure completion. First, the enhanced instance queries $\mathbf{Q}_{inst}^{''}$ interact with the multi-scale image features \mathbf{F}_{2D} via the *Instance-Image Cross-Attention* mechanism:

$$\mathbf{Q}_{inst}^{OD} = \text{DeformAttn}(\mathbf{Q}_{inst}^{''}, \mathbf{R}_{2D}, \mathbf{F}_{2D}) \quad (8)$$

This step enables the instance queries—updated by the visible region prediction in VD—to aggregate additional semantic cues from the image, preparing for the completion of occluded regions. The voxel embeddings from the visible region \mathbf{F}_{vis}^{VD} are first remapped to the entity space using the occupancy mask \mathbf{M} through the IndexBack operation, yielding \mathbf{E}_{occ} :

$$\mathbf{E}_{occ} = \text{IndexBack}(\mathbf{F}_{vis}^{VD}, \mathbf{M}) \quad (9)$$

Subsequently, \mathbf{E}_{occ} is flattened and interacts via *Scene-Instance Cross-Attention*, integrating semantic priors from the visible region into the occluded voxels. To enhance structural consistency, the OD module employs the *Scene Self-Attention* mechanism. This leverages the \mathbf{R}_{3D} to perform deformable self-attention over the occluded voxel embeddings, ensuring coherent geometric completion. Finally, in the *Scene Embedding Cross-Attention*, the class-level embedding \mathbf{C}_{od} interacts with the voxel features using a DETR-style attention module, which is consistent with the design of the Visible Embedding Cross-Attention. This process fuses the scene priors, simultaneously enhancing positional awareness and structural consistency. The OD module then outputs the fully refined voxel features \mathbf{F}_{occ}^{OD} , and subsequently generates the complete-scene semantic voxel prediction through the segmentation head.

F. Loss Functions

In the VOIC framework, the total loss is composed of the losses from the Visible Decoder (VD) and the Occlusion Decoder (OD):

$$L_{\text{total}} = L_{VD} + L_{OD} \quad (10)$$

where the losses of VD and OD share a unified structure:

$$L_X = \lambda_{\text{scal}} L_{\text{scal}}^{\text{geo}} + \lambda_{\text{ce}} L_{\text{ce}} + \lambda_{\text{miou}} L_{\text{miou}}, \quad X \in \{\text{VD}, \text{OD}\} \quad (11)$$

The components of the loss are defined as follows:

- $L_{\text{scal}}^{\text{geo}}$ [1] and L_{ce} [7] are employed to supervise geometric affinity and semantic prediction, respectively.
- L_{miou} is the semantic mIoU loss, formulated as

$$L_{\text{miou}} = 1 - \text{IoU}_{\text{mean}} \quad (12)$$

where IoU_{mean} denotes the mean intersection-over-union across all semantic classes.

IV. EXPERIMENTS

In this section, we present the experimental evaluations of our proposed method on the SemanticKITTI [8] and SSCBench-KITTI-360 [9] datasets. Comparative results against existing state-of-the-art approaches are provided in Sec. IV-C, while comprehensive ablation studies are reported in Sec. IV-D to further analyze the effectiveness of each component.

A. Dataset and Metric

We conduct experiments on the SemanticKITTI [8] and SSCBench-KITTI-360 [9] datasets, both of which offer densely annotated urban driving scenes derived from the KITTI Odometry Benchmark. The scenes are voxelized into grids of size $256 \times 256 \times 32$, covering a spatial volume of $51.2\text{m} \times 51.2\text{m} \times 6.4\text{m}$ with a voxel size of 0.2m .

SemanticKITTI contains 10 training sequences, 1 validation sequence, and 11 hidden test sequences. It provides RGB images with a resolution of 1226×370 and includes 20 semantic classes. SSCBench-KITTI-360 provides 7 training sequences, 1 validation sequence, and 1 test sequence, offering RGB images of size 1408×376 and defining 19 semantic classes.

In our camera-only setting, RGB images serve as the sole input modality. We follow standard SSC evaluation protocols and report Intersection over Union (IoU) and mean IoU (mIoU). IoU assesses binary occupancy (empty vs. occupied) and reflects geometric reconstruction performance, whereas mIoU evaluates per-class semantic accuracy—the primary metric in most SSC benchmarks [1] [7] [6] [31].

B. Implementation Details

We train our model on two RTX A6000 GPUs with a batch size of 1. Random horizontal flipping [36] [37] [38] and color jittering (brightness in the range $[1.2, 1.25]$, contrast in the range $[0.6, 0.65]$, and saturation adjustment of 0.1) are applied as image augmentation methods.

Depth information is obtained from MobileStereo [39] predictions, which are used as input to the model to enhance geometric reasoning.

Training is performed using the AdamW [40] optimizer with an initial learning rate of 3.5×10^{-4} , a weight decay of 0.015, and momentum coefficients $(\beta_1, \beta_2) = (0.9, 0.99)$. The loss

TABLE I

QUANTITATIVE RESULTS ON THE SEMANTICKITTI HIDDEN TEST SET. ^T REPRESENTS THE USE OF MULTI-FRAME INPUT. [†] REPRESENTS THE USE OF MULTI-CAMERA IMAGES AS INPUT. THE BEST AND THE SECOND BEST RESULTS ARE MARKED IN **BOLD** AND UNDERLINED, RESPECTIVELY.

Method	IoU	mIoU	Category IoU (%)																		
			road (15.30%)	sidewalk (11.13%)	parking (11.12%)	other-ground (0.56%)	building (14.1%)	car (3.93%)	truck (0.16%)	bicycle (0.03%)	motorcycle (0.03%)	other-veh. (0.20%)	vegetation (0.93%)	trunk (0.51%)	terrain (0.17%)	person (0.07%)	bicyclist (0.03%)	motorcyclist (0.59%)	fence (0.29%)	pole (0.29%)	traj-sign (0.08%)
MonoScene [1]	34.16	11.08	54.7	27.1	24.8	5.7	14.4	18.8	3.3	0.5	0.7	4.4	14.9	2.4	19.5	1.0	1.4	0.4	11.1	3.3	2.1
TPVFormer ^T [21]	34.25	11.26	55.1	27.2	27.4	6.5	14.8	19.2	3.7	1.0	0.5	2.3	13.9	2.6	20.4	1.1	2.4	0.3	11.0	2.9	1.5
VoxFormer ^T [6]	43.21	13.41	54.1	26.9	25.1	7.3	23.5	21.7	3.6	1.9	1.6	4.1	24.4	8.1	24.2	1.6	1.1	0.0	13.1	6.6	5.7
OccFormer [19]	34.53	12.32	55.9	30.3	31.5	6.5	15.7	21.6	1.2	1.5	1.7	3.2	16.8	3.9	21.3	2.2	1.1	0.2	11.9	3.8	3.7
NDC-Scene [20]	33.87	11.55	56.2	28.7	28.0	5.6	15.8	19.7	1.8	1.1	1.1	4.9	14.3	2.6	20.6	0.7	1.7	0.4	11.2	3.2	1.7
Symphonies [7]	42.19	15.04	58.4	29.3	26.9	11.7	24.7	23.6	3.2	3.6	2.6	5.6	24.0	10.0	23.1	3.2	1.9	2.0	16.1	7.7	8.0
SGN ^T [42]	45.42	15.76	60.4	31.4	28.9	8.7	28.4	25.4	4.5	0.9	1.6	3.7	27.4	<u>12.6</u>	28.4	0.5	0.3	0.1	18.1	10.0	8.3
MVFormer [29]	43.02	15.81	59.7	31.5	29.5	<u>12.5</u>	24.4	23.9	2.8	<u>3.7</u>	6.2	26.8	11.2	24.9	<u>3.1</u>	2.6	2.2	16.8	8.4	7.8	
CGFormer [43]	44.41	16.63	<u>64.3</u>	34.2	<u>34.1</u>	12.1	25.8	26.1	4.3	<u>3.7</u>	1.3	2.7	24.5	11.2	<u>29.3</u>	1.7	3.6	0.4	18.7	8.7	<u>9.3</u>
HTCL ^T [25]	44.23	<u>17.09</u>	64.4	<u>34.8</u>	33.8	<u>12.4</u>	25.9	<u>27.3</u>	<u>5.7</u>	1.8	2.2	5.4	25.3	10.8	31.2	1.1	<u>3.1</u>	0.9	21.1	9.0	8.3
VOIC(Ours)	45.69	17.42	63.2	35.7	36.0	7.2	<u>28.3</u>	27.4	<u>7.7</u>	4.4	4.7	<u>5.8</u>	<u>27.1</u>	12.8	28.3	2.5	0.0	0.2	<u>20.6</u>	<u>9.4</u>	9.7

TABLE II

QUANTITATIVE RESULTS ON THE SSCBENCH-KITTI360 TEST SET. ^T REPRESENTS THE USE OF MULTI-FRAME INPUT. [†] REPRESENTS THE USE OF MULTI-CAMERA IMAGES AS INPUT. THE BEST AND THE SECOND BEST RESULTS ARE MARKED IN **BOLD** AND UNDERLINED, RESPECTIVELY.

Method	IoU	mIoU	Category IoU (%)																	
			car (2.85%)	bicycle (0.01%)	motorcycle (0.00%)	truck (0.16%)	other-veh. (0.16%)	person (0.02%)	road (4.96%)	parking (2.51%)	sidewalk (0.43%)	other-grnd. (0.64%)	building (5.67%)	fence (0.96%)	vegetation (1.99%)	terrain (1.00%)	pole (0.22%)	traj-sign (0.52%)	other-struct. (0.28%)	other-obj. (0.58%)
MonoScene [1]	37.87	12.31	19.3	0.4	0.6	8.0	2.0	0.9	48.4	11.4	28.1	3.2	32.9	3.5	26.2	16.8	6.9	5.7	4.2	3.1
TPVFormer ^T [21]	40.22	13.64	21.6	1.1	1.4	8.1	2.6	2.4	53.0	12.0	31.1	3.8	34.8	4.8	30.1	17.5	7.5	5.9	5.5	2.7
OccFormer [19]	40.27	13.81	22.6	0.7	0.3	9.9	3.8	2.8	54.3	13.4	31.5	3.6	36.4	4.8	31.0	19.5	7.8	8.5	7.0	4.6
VoxFormer ^T [6]	38.76	11.91	17.8	1.2	0.9	4.6	2.1	1.6	47.0	9.7	27.2	2.9	31.2	5.0	29.0	14.7	6.5	6.9	3.8	2.4
Symphonies [7]	44.12	18.58	<u>30.0</u>	1.9	<u>5.9</u>	25.1	12.1	<u>8.2</u>	54.9	13.8	32.8	6.9	35.1	<u>8.6</u>	38.3	11.5	14.0	9.6	14.4	11.3
CGFormer [43]	48.07	<u>20.05</u>	29.85	<u>3.42</u>	3.96	17.59	6.79	6.63	63.85	17.15	40.72	5.53	42.73	8.22	38.8	24.94	16.24	<u>17.45</u>	10.18	6.77
SGN ^T [42]	47.06	18.25	29.0	3.4	2.9	10.9	5.2	3.0	58.1	<u>15.0</u>	36.4	4.4	42.0	7.7	38.2	<u>23.2</u>	<u>16.7</u>	16.4	9.9	5.8
VOIC(Ours)	48.18	21.37	30.9	4.4	<u>7.2</u>	<u>21.0</u>	<u>9.8</u>	8.4	62.6	11.9	41.3	<u>6.1</u>	43.5	<u>11.0</u>	38.9	22.7	17.2	20.1	<u>11.9</u>	9.2

TABLE III
COMPARISON OF INFERENCE TIME AND NUMBER OF PARAMETERS

Method	mIoU (%) [†]	Times (s) [↓]	Params (M) [↓]
MonoScene [1]	11.08	0.274	132.4
OccFormer [19]	13.46	0.338	203.4
VoxFormer [6]	13.35	0.256	57.9
Symphonize [7]	14.89	0.319	59.3
VOIC(Ours)	17.42	0.262	45.4

weights for both VD and OD are set as $\lambda_{\text{scal}} = 1$, $\lambda_{\text{ce}} = 1$, and $\lambda_{\text{miou}} = 10$.

Following other comparable methods [32] [7], the ResNet-50 [41] backbone and image encoder are initialized with pre-trained MaskDINO [33] weights.

A MultiStepLR scheduler is adopted, where the learning rate is decayed by a factor of 0.1 at epochs 12 and 23. The total training length is 35 epochs.

We set the input spatial voxel size to $128 \times 128 \times 16$ with $C = 128$ channels. The voxel representation is upsampled to $256 \times 256 \times 32$ using a 3D transposed convolution.

C. Main Results

Quantitative Results Table I presents a comparison of our proposed VOIC with other state-of-the-art camera-based SSC methods on the SemanticKITTI hidden test set. VOIC

outperforms existing approaches, establishing a new state-of-the-art. Compared to CGFormer, which also takes single-frame monocular images as input, our method achieves improvements of 0.79% in mIoU and 1.28% in IoU. These results validate the effectiveness of our approach in both geometric and semantic aspects. Notably, VOIC delivers top-tier performance on long-tailed categories, such as car, truck, bicycle, and motorcycle.

To further evaluate the effectiveness of VOIC across diverse scenarios, as shown in Table II, our method demonstrates significant advantages in semantic and geometric analysis on the data-rich SSCBench-KITTI-360 benchmark. VOIC surpasses all published methods in both IoU and mIoU metrics, achieving the best performance across the majority of categories.

Furthermore, as detailed in Table III, we compare the inference time and number of parameters with other state-of-the-art methods on the SemanticKITTI validation set. Our method achieves state-of-the-art performance with 17.42% mIoU using only 45.4M parameters. VOIC also achieves comparable inference time while being more lightweight.

Qualitative Results To provide an intuitive demonstration of VOIC's performance, Figure 4 illustrates qualitative results on the SemanticKITTI validation set, comparing our method with Symphonize. The first row shows the input images, ground truth labels, and VRLE-GT, while the second row presents the outputs of Symphonize and VOIC on OD and

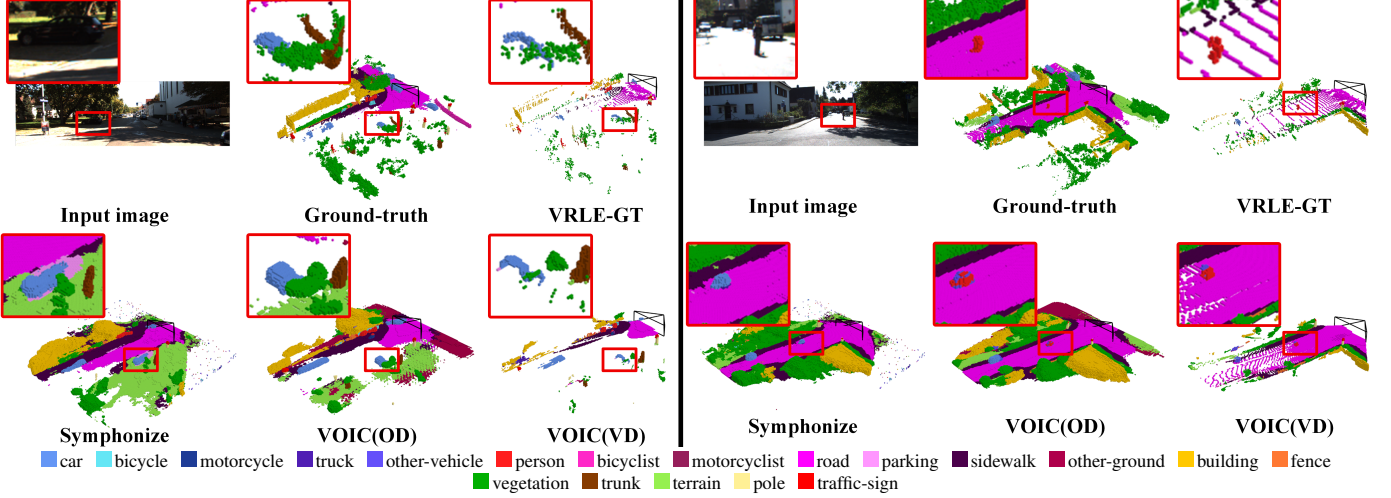


Fig. 4. Qualitative results on the SemanticKITTI validation set. VOIC enhances overall scene classification through high-quality visible-range semantic priors predicted by VD. Shown here is a comparison between VOIC and failure cases of Symphonize [7].

TABLE IV
ABLATION STUDY ON ARCHITECTURE, VRLE, AND 2D-TO-3D PROJECTION

Method	VRLE	2D-to-3D Projection	Decoder	IoU (%)	mIoU (%)
Baseline	\times	FLoSP	OD	36.86	11.09
1	\times	VEFC	OD	44.88	15.88
2	\times	VEFC	VD+OD	44.93	16.09
VOIC(Ours)	\checkmark	VEFC	VD+OD	46.44	17.64

VD, respectively. It can be observed that VD closely follows VRLE-GT, achieving more accurate semantic segmentation and occupancy information on visible objects. For example, in the first case, VOIC effectively captures the position and details of small objects such as cars, while in the second case, it accurately predicts pedestrian locations and guides OD accordingly.

D. Ablation Studies

To better understand the contributions of different components in VOIC, we conducted a series of ablation experiments, focusing on three aspects: the architectural design, the choice of 2D-to-3D projection methods, and the interaction flow between the Visible Decoder (VD) and the Occlusion Decoder (OD). All results are benchmarked on the SemanticKITTI validation set.

Ablation on the Architectural Components and Projection Method. Table IV summarizes the performance of VOIC under different architectural configurations. We first construct a Baseline model by removing the VRLE label, adopting FLoSP [1] as the 2D-to-3D projection module, and using OD as the final decoder, which yields 36.86% IoU and 11.09% mIoU.

Replacing FLoSP with the proposed VEFC module (Method 1), while still omitting VRLE and using only OD, improves performance to 44.88% IoU and 15.88% mIoU. This improvement arises from VEFC's depth-aware feature aggregation,

TABLE V
INTERACTION FLOW ABLATION

Method	Interaction Flow	IoU (%)	mIoU (%)
1	None	44.85	15.56
2	VD \rightarrow OD	45.33	17.02
VOIC(Ours)	VD \leftrightarrow OD	46.44	17.64

which provides more consistent geometric cues for semantic lifting.

Introducing the dual-decoder cascade VD+OD (Method 2), where VEFC is used but VRLE is still omitted and VD is supervised using the labels produced by OD, further improves performance to 44.93% IoU and 16.09% mIoU. This confirms that the structured interaction between VD and OD enhances the learning process even without visible-region supervision.

Finally, incorporating the VRLE label as explicit supervision for VD (VOIC, Ours) achieves the best results of 46.44% IoU and 17.64% mIoU. This progression demonstrates the crucial role of VRLE in enabling VD to progressively refine visible-region representations and produce a clear separation between visible and occluded region reconstruction.

Ablation on the Decoder Interaction Flow. Table V summarizes the effect of information exchange between VD and OD. When the two decoders are isolated, the model obtains 15.56% mIoU. Adding a unidirectional link from VD to OD raises the performance to 17.02% mIoU, indicating that visible-region features provide useful priors but a single forward fusion remains limited. Since VD guides OD through visible-region predictions, it naturally becomes necessary to propagate OD's global information back to VD to strengthen VD's feature learning, a capability absent in the unidirectional design. We therefore introduce a reverse link from OD to VD. This feedback brings OD's global context into VD, enabling mutual refinement and improving the final performance to 17.64% mIoU. Such bidirectional interaction allows both decoders to share complementary cues, benefiting full-scene reconstruction and reducing inconsistencies in the

visible regions.

V. CONCLUSION

In this paper, we introduced the Visible–Occluded Interactive Completion Network (VOIC), a novel two-stage framework for monocular 3D Semantic Scene Completion (SSC). Recognizing the distinct nature and information uncertainty between observed and occluded spaces, VOIC explicitly decouples the SSC task, moving beyond conventional unified decoding paradigms.

Our method is enabled by the Visible Region Label Extraction (VRLE) strategy, which generates precise, supervised labels for observed voxels, providing strong guidance for the Visible Decoder (VD). The VD accurately establishes high-fidelity semantic and geometric priors. Subsequently, the Occlusion Decoder (OD) leverages these priors to holistically infer the complete 3D scene, effectively resolving ambiguities in the occluded spaces through an interactive process.

Enhanced by a multi-level positional encoding mechanism for better geometric alignment, VOIC consistently achieved state-of-the-art performance on SemanticKITTI and SSCBench-KITTI-360. Notably, our framework achieved a geometric IOU of 45.69 and a semantic $mIoU$ of 17.42. By strategically separating visible perception from occluded completion, VOIC establishes a new, higher benchmark for accurate single-frame monocular SSC.

REFERENCES

- [1] A.-Q. Cao and R. De Charette, “Monoscene: Monocular 3d semantic scene completion,” in *Proceedings of the IEEE/CVF Conference on Computer Vision and Pattern Recognition*, 2022, pp. 3991–4001.
- [2] R. Cheng, C. Agia, Y. Ren, X. Li, and L. Bingbing, “S3cnet: A sparse semantic scene completion network for lidar point clouds,” in *Conference on Robot Learning*, 2021, pp. 2148–2161.
- [3] Z. Han, S. Li, X. Wang, X. Hu, R. Higashita, and J. Liu, “Multi-path sensory substitution device navigates the blind and visually impaired individuals,” *Displays*, p. 103200, 2025.
- [4] P. Li, R. Zhao, Y. Shi, H. Zhao, J. Yuan, G. Zhou, and Y.-Q. Zhang, “LODE: Locally Conditioned Eikonal Implicit Scene Completion from Sparse LiDAR,” in *2023 IEEE International Conference on Robotics and Automation (ICRA)*, 2023, pp. 8269–8276.
- [5] J. Lee, S. Lee, C. Jo, W. Im, J. Seon, and S.-E. Yoon, “Semicity: Semantic scene generation with triplane diffusion,” in *Proceedings of the IEEE/CVF Conference on Computer Vision and Pattern Recognition*, 2024, pp. 28337–28347.
- [6] Y. Li, Z. Yu, C. Choy, C. Xiao, J. M. Alvarez, S. Fidler, C. Feng, and A. Anandkumar, “Voxformer: Sparse voxel transformer for camera-based 3d semantic scene completion,” in *Proceedings of the IEEE/CVF Conference on Computer Vision and Pattern Recognition*, 2023, pp. 9087–9098.
- [7] H. Jiang, T. Cheng, N. Gao, H. Zhang, T. Lin, W. Liu, and X. Wang, “Symphonize 3d semantic scene completion with contextual instance queries,” in *Proceedings of the IEEE/CVF Conference on Computer Vision and Pattern Recognition*, 2024, pp. 20258–20267.
- [8] J. Behley, M. Garbade, A. Milioto, J. Quenzel, S. Behnke, C. Stachniss, and J. Gall, “Semantickitti: A dataset for semantic scene understanding of lidar sequences,” in *Proceedings of the IEEE/CVF International Conference on Computer Vision*, 2019, pp. 9297–9307.
- [9] Y. Li, S. Li, X. Liu, M. Gong, K. Li, N. Chen, Z. Wang, Z. Li, T. Jiang, and F. Yu, “Sscbench: A large-scale 3d semantic scene completion benchmark for autonomous driving,” in *2024 IEEE/RSJ International Conference on Intelligent Robots and Systems (IROS)*, 2024, pp. 13333–13340.
- [10] S. Song, F. Yu, A. Zeng, A. X. Chang, M. Savva, and T. Funkhouser, “Semantic scene completion from a single depth image,” in *Proceedings of the IEEE Conference on Computer Vision and Pattern Recognition*, 2017, pp. 1746–1754.
- [11] X. Chen, K.-Y. Lin, C. Qian, G. Zeng, and H. Li, “3d sketch-aware semantic scene completion via semi-supervised structure prior,” in *Proceedings of the IEEE/CVF Conference on Computer Vision and Pattern Recognition*, 2020, pp. 4193–4202.
- [12] J. Li, Y. Liu, D. Gong, Q. Shi, X. Yuan, C. Zhao, and I. Reid, “Rgbd based dimensional decomposition residual network for 3d semantic scene completion,” in *Proceedings of the IEEE/CVF Conference on Computer Vision and Pattern Recognition*, 2019, pp. 7693–7702.
- [13] P. Zhang, W. Liu, Y. Lei, H. Lu, and X. Yang, “Cascaded context pyramid for full-resolution 3d semantic scene completion,” in *Proceedings of the IEEE/CVF International Conference on Computer Vision*, 2019, pp. 7801–7810.
- [14] X. Wang, Z. Zhu, W. Xu, Y. Zhang, Y. Wei, X. Chi, Y. Ye, D. Du, J. Lu, and X. Wang, “Openoccupancy: A large scale benchmark for surrounding semantic occupancy perception,” in *Proceedings of the IEEE/CVF International Conference on Computer Vision*, 2023, pp. 17850–17859.
- [15] L. Roldao, R. De Charette, and A. Verroust-Blondet, “Lmscnet: Lightweight multiscale 3d semantic completion,” in *2020 International Conference on 3D Vision (3DV)*, 2020, pp. 111–119.
- [16] X. Yan, J. Gao, J. Li, R. Zhang, Z. Li, R. Huang, and S. Cui, “Sparse single sweep lidar point cloud segmentation via learning contextual shape priors from scene completion,” in *Proceedings of the AAAI Conference on Artificial Intelligence*, vol. 35, 2021, pp. 3101–3109.
- [17] X. Chang, H. Pan, W. Sun, and H. Gao, “A multi-phase camera-LiDAR fusion network for 3D semantic segmentation with weak supervision,” *IEEE Transactions on Circuits and Systems for Video Technology*, vol. 33, no. 8, pp. 3737–3746, 2023.
- [18] Z. Lu, B. Cao, and Q. Hu, “LiDAR-camera continuous fusion in voxelized grid for semantic scene completion,” *IEEE Transactions on Circuits and Systems for Video Technology*, 2024.
- [19] Y. Zhang, Z. Zhu, and D. Du, “Occformer: Dual-path transformer for vision-based 3d semantic occupancy prediction,” in *Proceedings of the IEEE/CVF International Conference on Computer Vision*, 2023, pp. 9433–9443.

[20] J. Yao, C. Li, K. Sun, Y. Cai, H. Li, W. Ouyang, and H. Li, “Ndcs-
scene: Boost monocular 3d semantic scene completion in normalized
device coordinates space,” in *2023 IEEE/CVF International Conference
on Computer Vision (ICCV)*, 2023, pp. 9421–9431.

[21] Y. Huang, W. Zheng, Y. Zhang, J. Zhou, and J. Lu, “Tri-perspective view
for vision-based 3d semantic occupancy prediction,” in *Proceedings of
the IEEE/CVF Conference on Computer Vision and Pattern Recognition*,
2023, pp. 9223–9232.

[22] S. Wang, J. Yu, W. Li, W. Liu, X. Liu, J. Chen, and J. Zhu, “Not all
voxels are equal: Hardness-aware semantic scene completion with self-
distillation,” in *Proceedings of the IEEE/CVF Conference on Computer
Vision and Pattern Recognition*, 2024, pp. 14 792–14 801.

[23] H. Xiao, H. Xu, W. Kang, and Y. Li, “Instance-aware monocular 3D
semantic scene completion,” *IEEE Transactions on Intelligent Trans-
portation Systems*, vol. 25, no. 7, pp. 6543–6554, 2024.

[24] M. Wang, Y. Ding, Y. Liu, Y. Qin, R. Li, and Z. Tang, “Mixssc: Forward-
backward mixture for vision-based 3d semantic scene completion,” *IEEE
Transactions on Circuits and Systems for Video Technology*, 2025.

[25] B. Li, J. Deng, W. Zhang, Z. Liang, D. Du, X. Jin, and W. Zeng,
“Hierarchical Temporal Context Learning for Camera-Based Semantic
Scene Completion,” in *Computer Vision – ECCV 2024*, A. Leonardis,
E. Ricci, S. Roth, O. Russakovsky, T. Sattler, and G. Varol, Eds., Cham,
2025, vol. 15062, pp. 131–148.

[26] J. Lin, J. Zhou, W. Xu, R. Xu, C. Wang, S. Chen, K. Fu, Y. Shao, L. Guo,
and S. Xu, “CurriFlow: Curriculum-Guided Depth Fusion with Optical
Flow-Based Temporal Alignment for 3D Semantic Scene Completion,”
Oct. 2025.

[27] H. Lu, Y. Su, X. Zhang, and H. Hu, “One Step Closer: Creating the
Future to Boost Monocular Semantic Scene Completion,” Jul. 2025.

[28] S. Chen, W. Sui, B. Zhang, Z. Boukhers, J. See, and C. Yang,
“Unleashing Semantic and Geometric Priors for 3D Scene Completion,”
Aug. 2025.

[29] F. Gao, Y. Chen, K. Wang, P. Zhou, and J. Lu, “MVFormer: UNet-like
Transformer with Mix-Voxel Attention for Camera-Based 3D Semantic
Scene Completion,” *IEEE Transactions on Circuits and Systems for
Video Technology*, 2025.

[30] D.-H. Pham, D.-D. Nguyen, A. Pham, T. Ho, P. Nguyen, K. Nguyen,
and R. Nguyen, “Semi-supervised 3D Semantic Scene Completion with
2D Vision Foundation Model Guidance,” in *Proceedings of the AAAI
Conference on Artificial Intelligence*, vol. 39, 2025, pp. 6514–6522.

[31] Z. Yang and Y. Peng, “SPHERE: Semantic-PHysical Engaged REpre-
sentation for 3D Semantic Scene Completion,” in *Proceedings of the
33rd ACM International Conference on Multimedia*, Dublin Ireland, Oct.
2025, pp. 7681–7690.

[32] Y.-W. Tseng, S.-P. Yang, J.-C. Wu, I.-B. Liao, Y.-H. Li, H.-H. Shuai, and
W.-H. Cheng, “Memory-Augmented Re-Completion for 3D Semantic
Scene Completion,” in *Proceedings of the AAAI Conference on Artificial
Intelligence*, vol. 39, 2025, pp. 7446–7454.

[33] F. Li, H. Zhang, H. Xu, S. Liu, L. Zhang, L. M. Ni, and H.-Y.
Shum, “Mask dino: Towards a unified transformer-based framework for
object detection and segmentation,” in *Proceedings of the IEEE/CVF
Conference on Computer Vision and Pattern Recognition*, 2023, pp.
3041–3050.

[34] X. Zhu, W. Su, L. Lu, B. Li, X. Wang, and J. Dai, “Deformable DETR:
Deformable Transformers for End-to-End Object Detection,” Mar. 2021.

[35] L.-C. Chen, G. Papandreou, I. Kokkinos, K. Murphy, and A. L. Yuille,
“DeepLab: Semantic image segmentation with deep convolutional nets,
atrous convolution, and fully connected crfs,” *IEEE transactions on
pattern analysis and machine intelligence*, vol. 40, no. 4, pp. 834–848,
2017.

[36] Y. Zhang, Z. Zhu, W. Zheng, J. Huang, G. Huang, J. Zhou, and J. Lu,
“Beverse: Unified perception and prediction in birds-eye-view for vision-
centric autonomous driving,” *arXiv preprint arXiv:2205.09743*, 2022.

[37] Y. Li, Z. Ge, G. Yu, J. Yang, Z. Wang, Y. Shi, J. Sun, and Z. Li,
“Bevdepth: Acquisition of reliable depth for multi-view 3d object detec-
tion,” in *Proceedings of the AAAI Conference on Artificial Intelligence*,
vol. 37, 2023, pp. 1477–1485.

[38] J. Huang, G. Huang, Z. Zhu, Y. Ye, and D. Du, “BEVDet: High-
performance Multi-camera 3D Object Detection in Bird-Eye-View,” Jun.
2022.

[39] F. Shamsafar, S. Woerz, R. Rahim, and A. Zell, “Mobilestereonet:
Towards lightweight deep networks for stereo matching,” in *Proceedings
of the Ieee/Cvf Winter Conference on Applications of Computer Vision*,
2022, pp. 2417–2426.

[40] I. Loshchilov and F. Hutter, “Decoupled Weight Decay Regularization,”
Jan. 2019.

[41] K. He, X. Zhang, S. Ren, and J. Sun, “Deep residual learning for image
recognition,” in *Proceedings of the IEEE Conference on Computer Vision
and Pattern Recognition*, 2016, pp. 770–778.

[42] J. Mei, Y. Yang, M. Wang, J. Zhu, J. Ra, Y. Ma, L. Li, and Y. Liu,
“Camera-based 3d semantic scene completion with sparse guidance
network,” *IEEE Transactions on Image Processing*, 2024.

[43] Z. Yu, R. Zhang, J. Ying, J. Yu, X. Hu, L. Luo, S.-Y. Cao, and H.-
L. Shen, “Context and geometry aware voxel transformer for semantic
scene completion,” *Advances in Neural Information Processing Systems*,
vol. 37, pp. 1531–1555, 2024.